ACS OMEGA

http://pubs.acs.org/journal/acsodf
Article

Enhanced Electrochemical Performance of MWCNT-Assisted Molybdenum−Titanium Carbide MXene as a Potential Electrode Material for Energy Storage Application

M. Waqas Hakim, Irfan Ali, Sabeen Fatima, Hu Li, Syed Hassan Mujtaba Jafri, and Syed Rizwan*

Cite This: *ACS Omega* 2024, 9, 8763−8772

ABSTRACT: Two-dimensional (2D) materials such as MXenes have attracted considerable attention owing to their enormous potential for structural flexibility. Here, we prepared a $Mo_2TiC_2T_x$-layered structure from parent $Mo_2TiAlC_2T_x$ MAX by chemically selective etching of the aluminum layer. The prepared MXene was employed in composite formation with CTAB-grafted multiwalled carbon nanotubes (MWCNTs) to have a structure with improved electrochemical performance. The samples were characterized to analyze the structure, morphology, elemental detection, vibrational modes, and surface chemistry, followed by an electrochemical performance of the $Mo_2TiC_2T_x$ MXene and MWCNTs@$Mo_2TiC_2T_x$ composite using the GAMRAY Potentiostat under a 1 M KOH electrolyte. The specific capacitance of pristine $Mo_2TiC_2T_x$ was 425 F g^{-1}, which was enhanced to 1740 F g^{-1} (almost 4 times) at 5 mV s^{-1} due to the increase in active surface area and conductive paths between the MXene sheets. The charge storage mechanism was studied by further resolving the cyclic voltammograms. MWCNTs@$Mo_2TiC_2T_x$ showed much improved electrochemical performance and reaction kinetics, making it an ideal material candidate for supercapacitor applications.

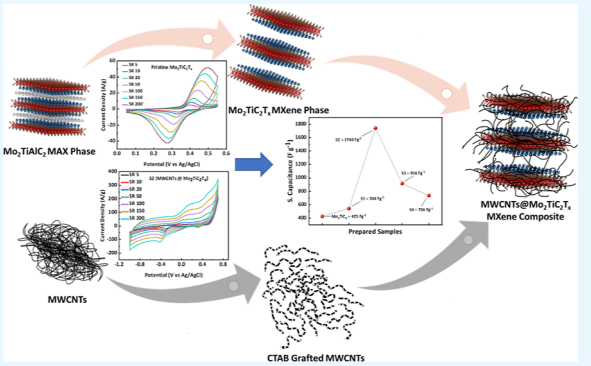

INTRODUCTION

With the growing world needs, energy consumption is also increasing, and with the emerging advanced electronics, the storage of energy is becoming critically important.[1] For this, researchers are working to find improved and efficient methods for higher energy storage. Supercapacitors have been a vital candidate for energy storage for many decades.[2] Scientists are working on various ways to enhance their storage capacity, lifetime, and recyclability. In the modern age, flexible and wearable electronics are in demand due to which it is important to work on the materials that could play their role in creating compact and foldable supercapacitor technology.[3] The storage capacity usually depends on the efficient adsorption of electrolytic ions over the electrode surface.[4,5] So, if the electrode has enough surface with active sites to interact with the electrolytic ions, the storage capacity will be increased. Two-dimensional (2D) materials have been playing their role in providing enough surface area to fabricate high-storage supercapacitors for many decades.[6−9] Also, their high flexibility paved a pathway toward flexible energy storage applications.[10−12]

Recently introduced MXene is a 2D water-attracting nanomaterial characterized by the general formula $M_{n+1}X_nT_x$. It is composed of n + 1 layers of early transition metal elements from groups 3−6, separated by n layers of carbon or nitrogen atoms. The surface terminations, such as −F, −OH, and −O, are indicated by T_x. $Ti_3C_2T_x$, the pioneering member of the MXene family, has been explored in diverse fields and for an array of applications.[13−16] Their metallic nature along with increased package density as well as pseudocapacitive behavior helps in enhancing the gravimetric as well as the volumetric capacitance of the devices.[17−19] Molybdenum-based MXene and other types of single- and double-transition metal carbide MXene phases have been studied for a variety of applications including electrocatalysts for water splitting application,[20] electromagnetic interference (EMI) shielding,[21] and electrochemical energy storage[22−25] and show relatively stable properties as compared to other MXene phases. Even though MXenes are a relatively newer class of materials, they still hold remarkable properties in many practical applications. The loss of the properties of MXenes is mainly due to the loss of their two-dimensional nature. MXene in its pristine form is subjected to the phenomenon of restacking which is intrinsic

Received: July 11, 2023
Revised: September 4, 2023
Accepted: October 11, 2023
Published: February 14, 2024

https://doi.org/10.1021/acsomega.3c04932
ACS Omega 2024, 9, 8763−8772

to the nature of MXenes; as the sheets of MXene are separated by the intercalation of water molecules in between their sheets which holds them apart, drying or evaporation of water molecules are the main causes of restacking.[26−30] As a result, MXene in its bare form is unable to utilize its full electrochemical active surface for energy storage.[31] To overcome this hurdle, researchers are introducing various methods of intercalation in between the MXene sheets as well as their hybrid or composite structure formation to forbid the process of restacking so that they could utilize it completely for charge storage.[23,32−36]

Carbon nanotubes (CNTs), an allotrope of carbon, have properties that enable them to be used inside energy conversion systems by enhancing the overall conductivity of the material by providing conductive channels throughout the material.[37] Their unique features like conductivity as well as tensile strength support their role inside the fields of sensors,[38] fuel cells,[39] metal-ion batteries,[40,41] and supercapacitors.[42] CNTs have also been used for synthesizing composite structures with other materials to enhance their storage capacity as electrodes inside supercapacitors.[43] By combining MXene with the CNTs, extraordinary supercapacitive properties can be achieved toward flexible energy storage applications. Many studies have been published depicting that CNTs in combination with MXene provide efficient electrodes for enhanced charge storage.[33,35] Recently, single-wall CNT/MXene ($Ti_3C_2T_x$) composites have been reported with a high volumetric capacitance of 2400 F g^{-1} at a scan rate of 2 mV s^{-1}.[44] Also, the V_2CT_x/CNTs composite showed a higher storage capacity of 1842 F g^{-1} at a scan rate of 2 mV s^{-1}.[45] The Mo_2TiC_2 MXene phase has been rarely explored in the field of energy storage, and according to a report on Li-ion batteries, it achieved 1.7 times higher capacity than other multilayered MXene forms.[46]

Here in this report, we used the double-transition metal MXene ($Mo_2TiC_2T_x$) and then synthesized its composites with multiwall carbon nanotubes (MWCNTs) to see their role as electrode material inside the supercapacitors, which is to our knowledge the very first report of energy storage for this MXene phase and MWCNTs. The structural and morphological properties are also explored to see the crystallinity and uniformity of the structures. To observe the morphology of the prepared samples, the material is characterized using SEM and HRTEM. Further different spectral modes and the effect of composite formation of functional groups have been evaluated using RAMAN and XPS analyses. The composites provided ultrahigh charge storage for the fabricated supercapacitor electrode.

RESULTS AND DISCUSSION

For the structural and crystallographic analyses of the synthesized material, we have performed X-ray diffraction (XRD) analysis of the Mo_2TiAlC_2 MAX phase, Mo_2TiC_2-etched MXene, MWCNTs, and the synthesized composites. Figure 1 shows the XRD plots of the synthesized materials. MAX to MXene transition after the 50% hydrofluoric acid (HF) etching shows the shifting of the (002) peak; this shifting from 9.4° 2θ to 6.55° 2θ corresponds to the change of the c-lattice parameter (c-Lp) from 18.6 to 26.73 Å. This shift of peak to lower angle corresponds to good etching and agrees with the already reported data for this specific MXene.[14,47,48] The increase in the intensity and back-shifting of the (002) peak represent the opening in the hexagonal structure of

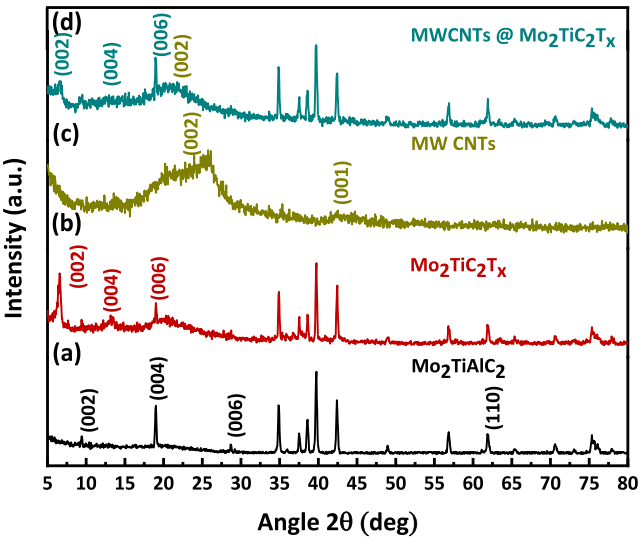

Figure 1. XRD pattern of (a) Mo_2TiAlC_2 MAX, (b) $Mo_2TiC_2T_x$ MXene etching using HF, (c) MWCNTs, and (d) S2 (MWCNTs@ $Mo_2TiC_2T_x$).

MXene, and the removal of the aluminum layer and the sharpness of the (002) peak represent the increase in the overall crystallinity and reduction of defects in the MXene structure. MWCNTs show prominent peaks at 25.75 and 42.5° 2θ, respectively, which correspond to (002) and (001) peaks of the hexagonal plane of graphite in carbon nanotube's structure (JCPDS no. 41-1487).[49] The XRD MWCNTs@$Mo_2TiC_2T_x$ composites show the (002) peak of $Mo_2TiC_2T_x$ MXene at a similar angle of 6.55° 2θ, and the downshifting of the (002) MWCNT peak to 20.8° 2θ corresponds to the successful formation of the composite. The hump-like presence of the (002) peak at 20.8° 2θ represents the presence of the MWCNT structure in a hybrid structure.

Structural, crystallinity, and phase transformational information on material was characterized using Raman spectroscopy analysis. Figure 2 shows the Raman spectrum for the prepared samples. Figure 2a represents the Raman spectra of Mo_2TiAlC_2 MAX which shows vibration corresponding to the structure and surface of flakes. The Mo_2TiAlC_2 bulk MAX phase shows a Raman peak at 160.47 cm^{-1}, which is assigned to the E_{2g} (in-plane) small displacement of Al atom. Similarly, peaks observed at 239.31, 299.6, and 408.45 cm^{-1} are all assigned to A_{1g} out-of-plane vibration and displacement of Al atom attached to Mo atom in the MAX phase.[50,51] In addition, peaks at 598.56 and 834.25 cm^{-1} are related to the A_{2g} out-of-plane vibration of Al atom in Mo−Al−Mo bonding.[52] After HF treatment, the Raman spectra of MXene in Figure 2b show the sharpening of Raman peaks, which shows the increase in crystallinity of the synthesized material.[53] The peak at 147.46 cm^{-1} is attributed to E_g in-plane vibration of Mo atom in the MXene flake. Peak at 279.4 cm^{-1} appears due to the B_{2g} and B_{3g} vibrations related to the O atom attached as a termination group to the MXene flake. Other vibration modes at 331.81, 376.34, and 605.47 cm^{-1} belong to the T_x-region of etched MXene and are assigned to E_g (in-plane) vibrations of Mo−$(O)_2$, Mo−$(OH)_2$, and A_{1g} (out-of-plane) vibrations of Mo−T_x, respectively. Raman peaks at 661.82, 818.24, and 989.71 are due to the presence of oxygen functionalization and are assigned to A_{1g}, B_{3g}, B_{1g}, and A_{1g}, respectively.[54]

https://doi.org/10.1021/acsomega.3c04932
ACS Omega 2024, 9, 8763−8772

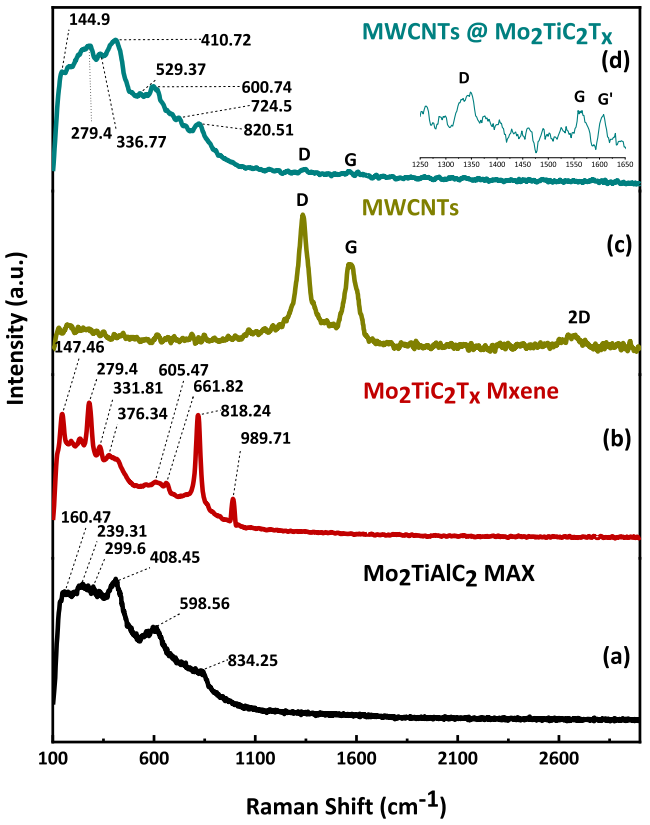

Figure 2. Raman spectrum of (a) Mo_2TIAlC_2 (312) MAX phase, (b) $Mo_2TiC_2T_x$ power MXene, (c) MWCNTs, and (d) MWCNTs@ $Mo_2TiC_2T_x$ composite with the inset showing the Raman shift region at 1200−1600 cm^{-1}.

Figure 2c shows the Raman spectra of MWCNTs; characteristics Raman bands were observed for D, G, D′, and 2D or D′ bands at 1334.46, 1564.51, and 1574.16 cm^{-1}, respectively.[55] The MWCNT@$Mo_2TiC_2T_x$ Raman spectrum is shown in Figure 2d; shifting peaks were observed when comparing it with pristine MXene spectra in Figure 2b. The peak at 147.46 downshifted to 144.9 cm^{-1} after composite formation, which is related to the E_g (in-plane) vibration of Mo atom. Downshifting of the Raman peak is associated with the material subjected to tensile stress, which can be due to the pressure caused by the presence of MWCNTs on the surface of MXene flakes. Another peak shift was observed from 331.81 to 336.77 cm^{-1} related to the E_g (in-plane) vibration of the Mo atom attached to the −OH functional group. This slight upshifting can be related to an increase in the bond length of change in the functional group. A peak at 605.47 cm^{-1} was downshifted to 600.74 cm^{-1} in MWCNTs@$Mo_2TiC_2T_x$ related to the A_{1g} (out-of-plane) vibration of the attached functional groups. Peak-related B_{1g} (Mo−O) upshifted from 818.24 to 820.51 cm^{-1}. Figure 2d represents the Raman spectra of the MWCNTs@$Mo_2TC_2T_c$ composite containing vibrational modes for both MXene and MWCNTs in the data. Raman peaks at lower wavenumbers are present due to vibrations caused by the Raman laser interaction with the structure of MXene. A D and G bands were observed at wavenumbers 1335.99 and 1558.05 cm^{-1}, respectively, because of the graphitic MWCNT structure along with the functional groups present on the surface of $Mo_2TiC_2T_x$. Furthermore, $\frac{I_D}{I_G}$ ratio for MWCNTs and prepared MWCNTs@$Mo_2TiC_2T_x$ composite was calculated, and the value decreased from 1.55 to 1.10, which shows the increase in the structural stability and decrease in the defects of the overall MWCNT structure.[60]

For the detailed elemental composition and surface study of the material, X-ray photoelectron spectroscopy (XPS) was conducted. Figure 3 shows the overall data for the XPS analysis. Figure 3a displays a comparison plot for both pristine $Mo_2TiC_2T_x$ and MWCNTs@$Mo_2TiC_2T_x$. Composite data shows the increase in the peak intensity in the region C 1s, which reveals the presence of MWCNTs on the surface of $Mo_2TiC_2T_x$ MXene. Data shows the possible termination groups −F, −OH, and −O as ($Mo_2TiC_2(OH)_2$), ($Mo_2TiC_2F_2$), or ($Mo_2TiC_2O_2$).[18] Figure 3b demonstrates

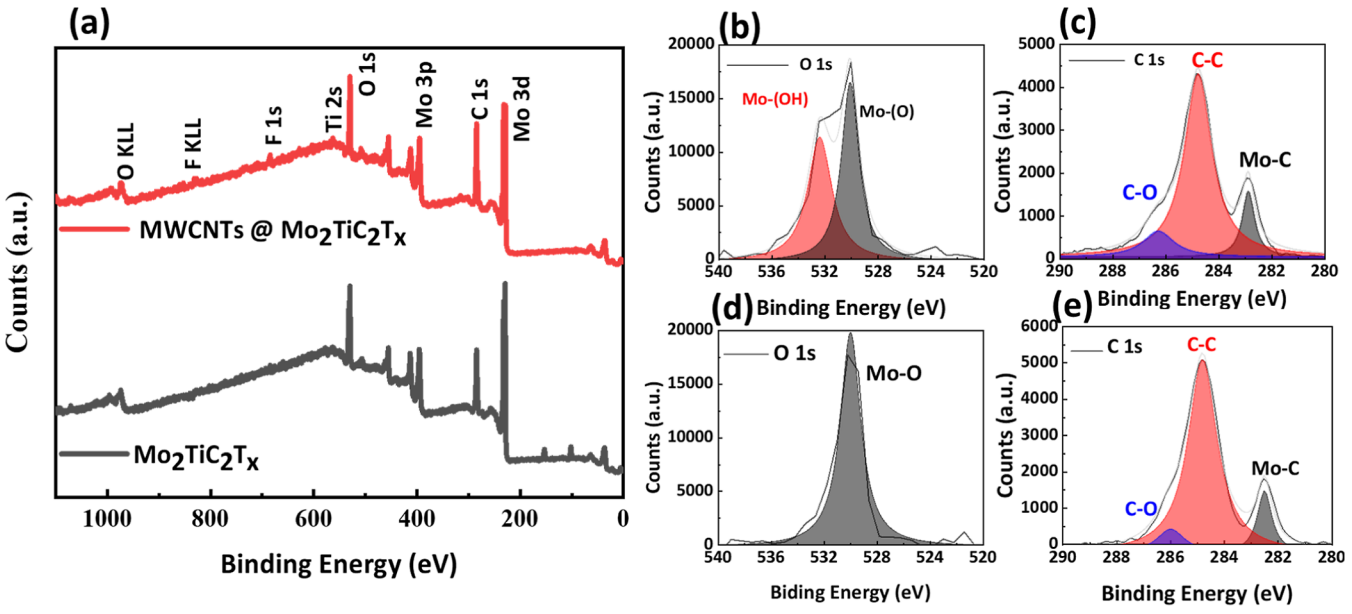

Figure 3. XPS analysis of $Mo_2TIC_2T_x$ and MWCNTs@$Mo_2TiC_2T_x$ MXene composite: (a) comparison plot for both samples; (b,c) high-resolution XPS spectrum in the region of O 1s and C 1s for $Mo_2TiC_2T_x$; and (d,e) O 1s and C 1s spectra for MWCNTs@$Mo_2TiC_2T_x$.

https://doi.org/10.1021/acsomega.3c04932
ACS Omega 2024, 9, 8763−8772

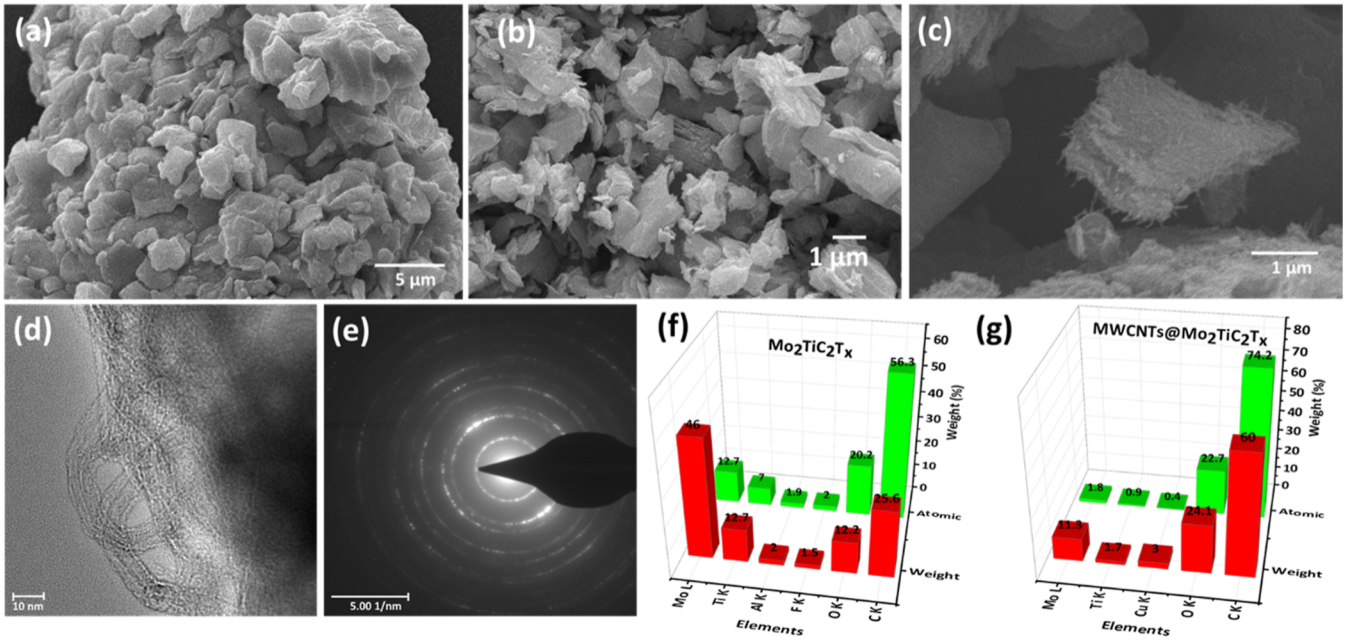

Figure 4. Electron microscopic images of prepared samples: (a) Mo_2TiAlC_2 MAX, (b) $Mo_2TiC_2T_x$ MXene, and (c) MWCNTs@$Mo_2TiC_2T_x$ composite; (d) HRTEM image of MWCNTs@$Mo_2TiC_2T_x$ composite; (e) selected area electron diffraction (SAED) pattern of MWCNTs@$Mo_2TiC_2T_x$ composite; (f) EDX of pristine MXene; and (g) EDX of MWCNTs@$Mo_2TiC_2T_x$ composite.

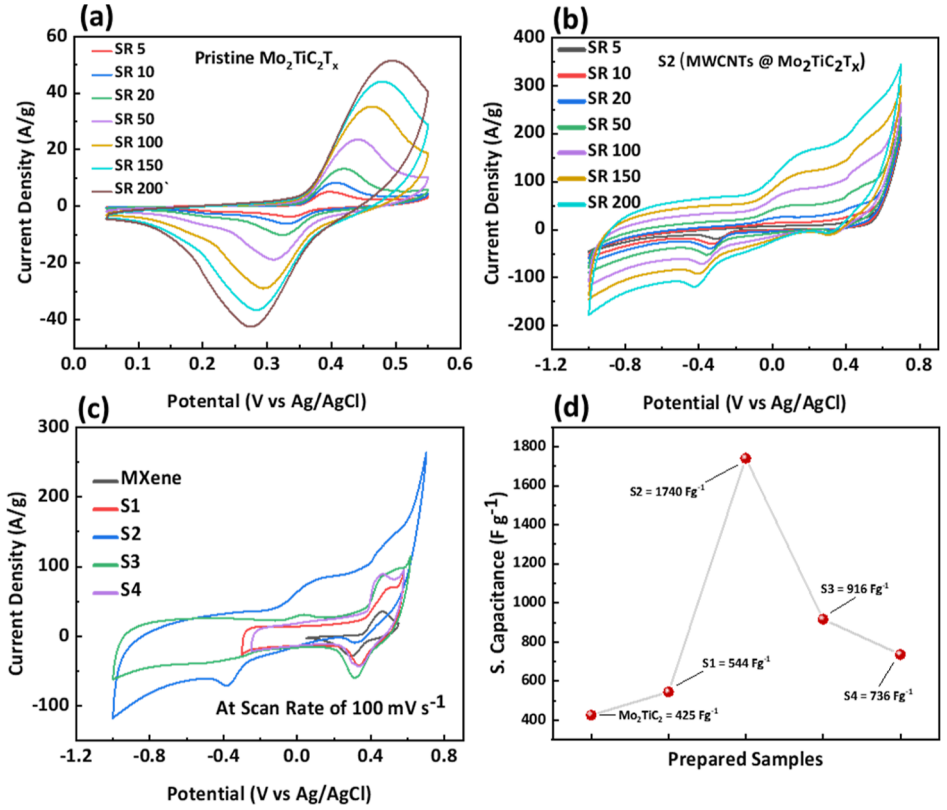

Figure 5. Electrochemical analysis of the prepared samples: (a) *CV* profile of $Mo_2TiC_2T_x$ pristine MXene; (b) *CV* profile of S2 (MWCNTs@$Mo_2TiC_2T_x$) composite; (c) *CV* curve comparison of all the samples prepared at 100 mV s^{-1}; (d) capacitance value comparison at 5 mV s^{-1}.

the high-resolution spectra in the region of O 1s of $Mo_2TiC_2T_x$; the data show the O−Mo bonding of the MXene surface atom and −OH bonding with the Mo atom at 530.17 and 532.37 eV, respectively.[56,57] Three XPS fitting peaks in the region of C 1s are presented in Figure 3c for $Mo_2TiC_2T_x$. The first peak at 282.89 eV is attributed to Mo−C bonding from within the structure of MXene, the second peak at 284.77 eV is associated with C−C bonding, and the peak at 286.34 is attributed to C−O.[58] Figure 3d shows that the high-resolution XPS peak fitting in the region of O 1s for

https://doi.org/10.1021/acsomega.3c04932
ACS Omega 2024, 9, 8763−8772

Table 1. Electrochemical Performance Comparison of MXene/CNT Structure and Similar Fabricated Electrode Materials

electrode material	configuration	electrolyte	findings	year	refs
MWCNTs-$Ti_3C_2T_x$@carbon cloth	3-electrode system	$Ni(NO_3)_2{\cdot}6H_2O$ and $Al(NO_3)_3{\cdot}9H_2O$ aqueous mixed electrolyte	114.58 mF cm^{-2}@1 mA cm^{-2}	2020	66
Nb_2CT_x/CNT/activated carbon	2-electrode system	1 M H_2SO_4	462.0 mF cm^{-2}@2 mV s^{-1}	2020	67
Ti_3C2T_x@/CNTs	3-electrode system	1 M H_2SO_4	423.4 F g^{-1}@1 A g^{-1}	2020	68
$Ti_3C_2T_x$/carbon nanofibers	3-electrode system	1 M H_2SO_4	120 F g^{-1}@2 mV s^{-1}	2021	69
MWCNTs/V_2CT_x	3-electrode system	1 M KOH	1842 F g^{-1}@2 mV s^{-1}	2022	70
$Ti_3C_2T_x$/CNTs/sodium hyaluronate	3-electrode System	1 M NaOH	13.95 ± 2.45 F cm^{-3}	2023	71
$Ti_3C_2T_x$/RGO/CNTs nanofilm	2-electrode system	1 M PVA/H_2SO_4	463.5 F g^{-1}@1 A g^{-1}	2023	72
MWCNTs@$Mo_2TiC_2T_x$	3-electrode system	1 M KOH	1740 F g^{-1}@5 mV s^{-1}	2023	this work

MWCNTs@$Mo_2TiC_2T_x$ data shows only one peak associated with Mo−O at 530.03 eV.[21] Fitting in the region of C 1s for MWCNTs@$Mo_2TiC_2T_x$ is shown in Figure 3e with three similar peaks observed in the data. Mo−C and C−O were observed at 282.52 and 286.03 eV, respectively. The C−C peak was observed at 284.83 eV. The increase in the intensity of the C−C peak in the data corresponds to the presence of MWCNTs on the surface of MXene.[59] Also, O 1s of MXene and MWCNTs@$Mo_2TiC_2T_x$, Figure 3b,d, show the absence of −OH functional group on the composite material and the attachment of MWCNTs with the oxygen functional group replacing the H atom, and the increase in the intensity of the C−C peak suggests the successful formation of $Mo_2TiC_2T_x$ and MWCNT composite.

Scanning electron microscopy (SEM) with energy-dispersive X-ray spectroscopy (EDX) was used for the morphological study and elemental detection with percentage concentration analysis. Figure 4 shows the SEM images, HRTEM images, and EDX spectra for the synthesized material. Bulk-sized Mo_2TiAlC_2 particle phase of the MAX SEM image is shown in Figure 4a after HF etching, and removal of A-layer $Mo_2TiC_2T_x$ shows the sheet nature of the material as shown in Figure 2b. The SEM image of the composite MWCNTs@$Mo_2TiC_2T_x$ prepared sample in Figure 4c shows the attached MWCNTs as a web which covers the whole structure of MXene. This combination of MXene and MWCNTs provides an improved conductive medium, which results in superior electrochemical performance.[40,61,62] High-resolution transmission electron microscopic image of MWCNTs@$Mo_2TiC_2T_x$ is shown in Figure 4d. The image shows a web of MWCNTs on the surface of MXene. The selective area electron diffraction (SAED) pattern of the composite material is shown in Figure 4e, showing the polycrystalline nature of the composite, where the innermost ring corresponds to the (002) plane of MXene. Composition and elemental concentration were analyzed using EDX analysis. Figure 4f shows the EDX spectra for $Mo_2TiC_2T_x$ MXene. The small concentration of aluminum in the MXene sample shows the effective removal of the A-layer from the MAX phase.[63] The presence of fluorine and oxygen shows that most of the functional groups attached are −F, −OH, and −O as already discussed in the XPS analysis. Figure 4g is the EDX spectrum of the prepared sample S2 (MWCNTs@$Mo_2TiC_2T_x$). The rise in the concentration of carbon in the sample shows the presence of MWCNTs in the prepared sample. The presence of MWCNTs on the surface of MXene sheets acts as a conductive channel which results in enhanced charge storage capabilities and charge transport behavior.[45]

For the electrochemical testing of the material, cyclic voltammetry (CV) and electrochemical impedance spectroscopy (EIS) are performed by using a three-electrode system. The working electrode was made by depositing the material under testing onto nickel foam; Ag/AgCl was used as a reference electrode, and a platinum wire was used as a counter electrode using 1 M KOH solution as an electrolyte because of its ionic conductivity and economic price, low toxicity, and nondamaging behavior toward the electrode material.[64,65] *CV* measurements were carried out for all the electrodes from the scan rate of 200 to 5 mV s^{-1}. Figure 5 shows the electrochemical data for the MXene and composite prepared. *CV* curves for pristine MXene powder were taken over the potential window of 0.05−0.55 V and are shown in Figure 5a. Improved electrochemical performance of an electrode was observed for MWCNTs@$Mo_2TiC_2T_x$ due to the addition of MWCNTs, which results in enhanced performance compared to that of pristine MXene. The addition of MWCNTs results in an increase in the available surface area, and the overall conductivity of the material *CV* data for the MWCNTs@$Mo_2TiC_2T_x$ composite (4:20) ratio is given in Figure 5b. A comparison of the *CV* curves for all the prepared samples is reported in Figure 5c and shows the change in the electrochemical behavior of the electrode with a change of ratio for the composite formation. At higher composite ratios, the surface of the MXene particle is fully covered with the web of MWCNTs resulting in the reduction of the energy storage property of the material. In Figure 5d, comparison of specific capacitance for each sample prepared is reported; at 5 mV s^{-1}, the specific capacitance of MXene was observed to be at 425 F g^{-1}; with the increase in the concentration of the MWCNTs, the specific capacitance of the electrode rises to a value of 1740 F g^{-1} for 2:10 (S2) MWCNTs@$Mo_2TiC_2T_x$ and then with the further increase in concentration-specific capacitance reduced to 736 F g^{-1} at a ratio of 1:2 for (S4) MWCNTs@$Mo_2TiC_2T_x$. Table 1 shows a generic comparison of the prepared electrode material (MWCNTs@MXene) with already published reports in the field of MXene supported by carbon-based structure in two- or three-electrode systems, and the data show the importance and high performance of the MWCNTs@Mo_2TiC2T_x electrode material in the field of supercapacitor applications.

https://doi.org/10.1021/acsomega.3c04932
ACS Omega 2024, 9, 8763−8772

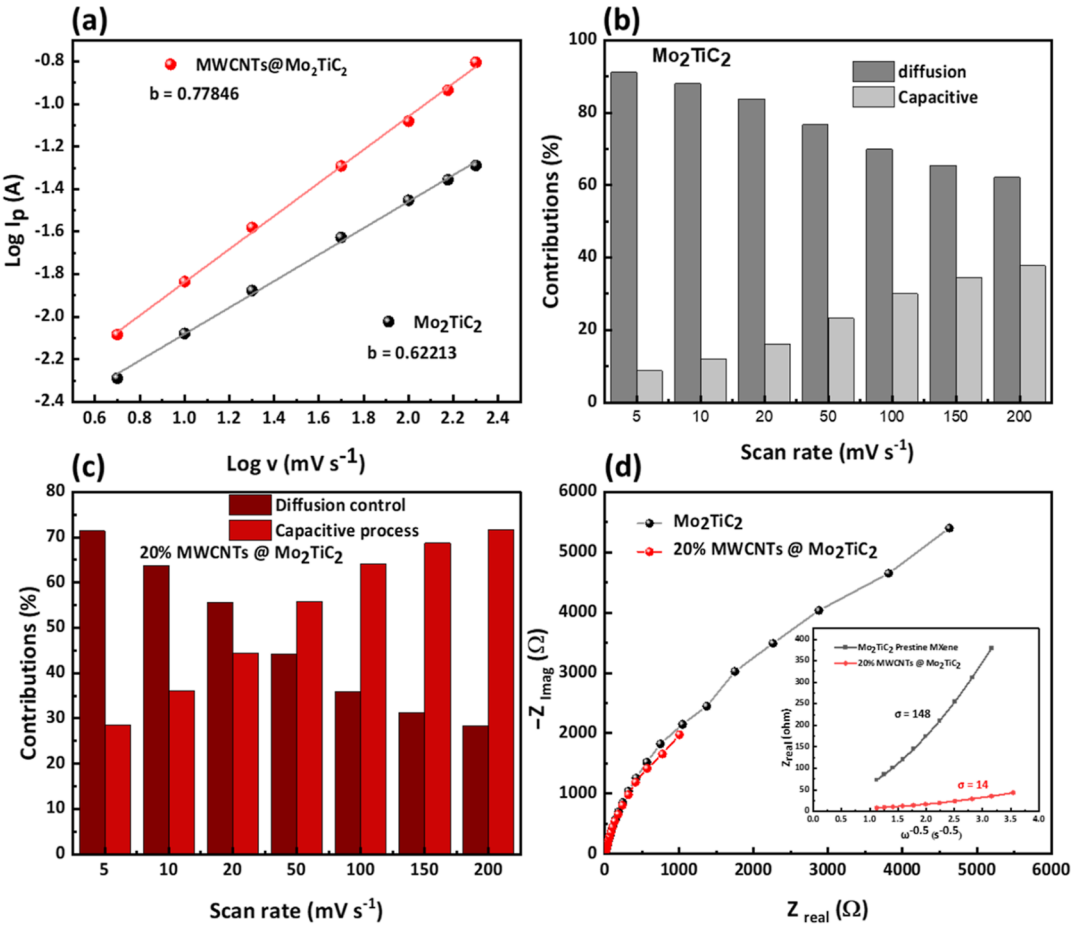

Figure 6. Charge storage mechanism and EIS analysis of $Mo_2TiC_2T_x$ and MWCNTs@$Mo_2TiC_2T_x$. (a) Log of peak current vs log of scan rate plot for both pristine $Mo_2TiC_2T_x$ MXene and MWCNTs@$Mo_2TiC_2T_x$ composite. (b) Capacitive-controlled and diffusive-controlled current contribution for pristine MXene. (c) Capacitive-controlled and diffusive-controlled current contribution for MWCNTs@$Mo_2TiC_2T_x$ composite electrode. (d) EIS spectrum of the materials with the inset plot for the demonstration of sigma value from the EIS data.

To study the kinetics of the electrode material, cyclic voltammogram curves are further resolved to get the nature of the types of contributions taking part in the capacitance with the change in scan rates. Generally, there are two types of charge storage contributions of an electrode following a faradaic charge storage mechanism: one is diffusion-controlled faradaic redox reaction and the other is a faradaic surface-controlled redox reaction (pseudocapacitive). From the *CV* profile, these two mechanisms can be separated to get a better understanding of the kinetics happening at the electrode surface.

The current at the electrode when a constant scan rate is used is controlled by the equation $i = av^b$, where i is the current, v is the scan rate, and a and b are the constants. The value of b is used to determine the nature of the charge storage mechanism. b value of 0.5 corresponds to the diffusion-controlled processes, and b value of 1 corresponds to the capacitive charge storage mechanism.[73] From Figure 5a,b, it can be seen that the *CV* curves of pristine MXene have dominated redox peaks, showing an increase in current with an increase in scan rate, which shows that the electrode has a more capacitive-controlled current contribution in the overall capacitance. The *CV* plots of the composite material show slightly more diffusive trends than the capacitive ones. Further, if we take the logarithm of the equation, we can write the equation as $\log i = b \log v + \log a$. The equation gets the form of a straight line equation, where b is the slope and can be calculated as shown in Figure 6a. In this work, the obtained b value for prestige $Mo_2TiC_2T_x$ was 0.62, and for the composite, we got the value of 0.77. This shifting of value toward 1 signifies that the charge storage mechanism for the composite is mainly due to the capacitive or surface-controlled reaction. The nature of the charge storage mechanism with changing scan rates for MXene and MWCNTs@$Mo_2TiC_2T_x$ is shown in Figure 6b,c. From the data, a trend can be seen, as for pristine MXene at higher scan rates, capacitive and diffusion-controlled processes are contributing side by side, but for the slower scan rate, diffusion-controlled processes are more dominant. Similarly, for MWCNTs@$Mo_2TiC_2T_x$ at higher scan rates, the main contribution is capacitive. At a slower scan rate, the composite electrode shows more contribution of diffusive-controlled processes.

Electrochemical impedance spectroscopy (EIS) analysis (Figure 6d) demonstrates the Nyquist plot to analyze the electrochemical response of both samples using nickel foam as a current collector in 1 M KOH solution as an electrolyte. The inset shows that the higher frequency region of EIS Nyquist data shows that the solution resistance R_s is the same for both pristine $Mo_2TiC_2T_x$ and MWCNTs@$Mo_2TiC_2T_x$ composite. The composite material shows lower electrode resistance as compared to the pristine MXene electrode. Figure 6d shows an inset plot between real impedance and inverse sqrt of

https://doi.org/10.1021/acsomega.3c04932
ACS Omega 2024, 9, 8763−8772

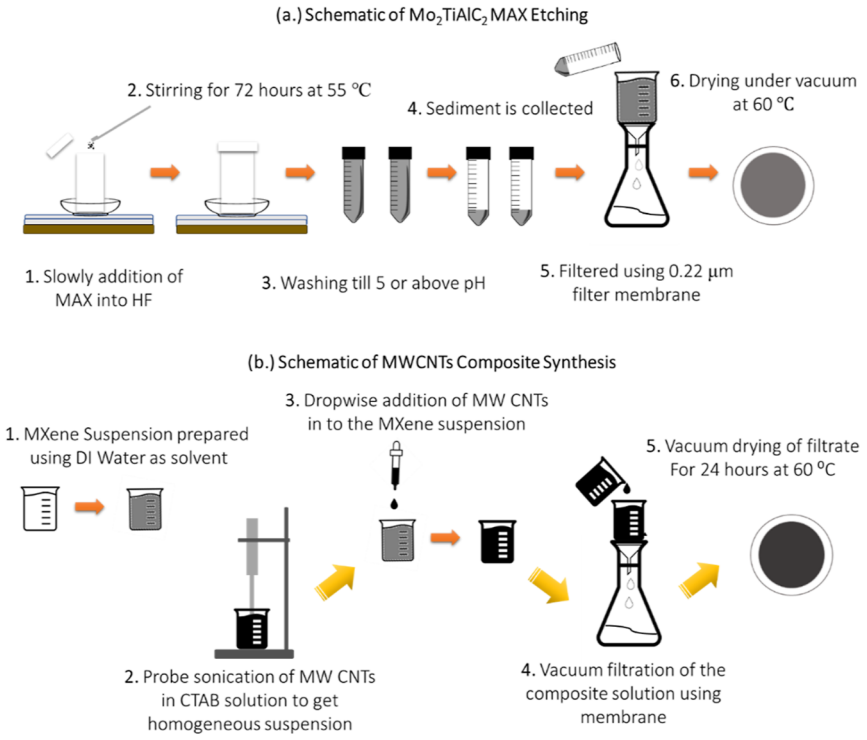

Figure 7. Schematic representation of (a) etching procedure for the synthesis of $Mo_2TiC_2T_x$ MXene. (b) MWCNTs@MXene composite synthesis.

frequency, a plot drawn to evaluate the value of σ, and a slope of the plotted data that belongs to the Warburg factor. The coefficient of diffusion for K^+ ions at a lower frequency can be calculated through σ value using eq 1.[35]

$$\sigma = A_w = \left(\frac{RT}{An^2F^2\Theta C\sqrt{2D}}\right) \quad (1)$$

where every term is constant except D, which has an inverse relation to the Warburg coefficient (σ). The value of σ changes from 32.91 to 5.23 for $Mo_2TiC_2T_x$ and MWCNTs@$Mo_2TiC_2T_x$ electrodes, respectively. This shows that the diffusion of electrolytic ions is more dominant in the composite material, which increases the electrochemical performance of the electrode material.[74,75]

CONCLUSIONS

To summarize, we have exhibited a straightforward method for the synthesis of 2D $Mo_2TiC_2T_x$ MXene with a high specific capacitance of 425 F g^{-1} at 5 mV s^{-1}. MWCNTs were used to further enhance the storage capacity of $Mo_2Ti_2T_x$ MXene by forming a weblike structure around MXene particles. A successful synthesis of the material is supported by XRD, XPS, and Raman spectroscopy. The composite material showed a high value of 1740 F g^{-1} specific capacitance at 5 mV s^{-1}. From the cyclic voltammetry plots, the b-value showed that pristine MXene shows the dominance of diffusion-controlled processes at lower scan rates after composite formation material shows a charge storage mechanism with the contribution of both capacitive and diffusion-controlled processes. Similarly, from the EIS data, the calculated σ value supports the CV data as the composite shows a higher value of diffusion coefficient compared to pristine $Mo_2TiC_2T_x$ MXene. The synthesized composite MWCNTs@$Mo_2TiC_2T_x$ shows a high capacitance and hence is a candidate for energy storage devices.

EXPERIMENTAL SECTION

Synthesis of Mo_2TiC_2 MXene Powder. Mo_2TiAlC_2, MAX powder was etched using HF as an etchant. 1 g of Mo_2TiAlC_2 was added to 10 mL of HF using an ice bath over the time scale of 10 min to minimize the localized heating effect. After the addition of MAX into the Teflon beaker with HF, the beaker was transferred onto the oil bath kept at 55 °C and kept there for 72 h with continuous stirring at 250 rpm using a Teflon-coated magnetic stirring bar. The mixture was then washed five times until the overall pH of the solution was above 5. For each cycle, 50 mL of DI water was used to centrifuge out the products from the etching reaction. Centrifugation was carried out at 3500 rpm, decanting supernatant every time. After the last centrifugation, sedimented MXene was mixed in 500 mL of DI water, then filtered on a nylon membrane filter of 0.22 μm pore size, and then vacuum-dried at 60 °C overnight. Schematics for the synthesis procedure are listed in Figure 7a.

Synthesis of MWCNTs@$Mo_2TiC_2T_x$. The composite was formed by making the dispersion of MWCNTs in DI water. The dispersion was obtained by grafting MWCNTs using cetyl-trimethyl ammonium bromide (CTAB). Initially, a 2 mM solution of CTAB in DI water was obtained. MWCNTs and CTAB solution were probe-sonicated for 1 h with a concentration of 5 mg of MWCNTs per 10 mL of CTAB solution. CTAB-grafted MWCNTs were added dropwise to the already prepared Mo_2TiC_2 suspension. The weight of Mo_2TiC_2 MXene was fixed to 100 mg for each sample prepared to keep the concentration of the dispersion at 1 mg per mL. Figure 7b shows a schematic diagram for the composite synthesis. The formed sample was then filtered using a nylon membrane and dried in an oven at 60 °C for 24 h. By following a similar protocol, samples with different ratios (1:20, 4:20, 7:20, and 10:20) were prepared and labeled S1, S2, S3, and S4, respectively.

https://doi.org/10.1021/acsomega.3c04932
ACS Omega 2024, 9, 8763−8772

Electrode Fabrication for Electrochemical Testing. The electrode for electrochemical characterization was made using a 1 × 1.5 cm piece of Ni foam. The cleaning process was performed on Ni foam by processing it with 1 M HCl and bath-sonicated for 15 min to remove the oxide layer if present, followed by 10 min bath sonication using ethanol and then DI water. The cleaned electrode is then dried at 60 °C until water is completely evaporated. The slurry for the deposition is prepared in two drops of (*n*-methyl-2-pyrrolidone) NMP as a solvent with the active material, carbon black, and (polyvinylidene fluoride or polyvinylidene difluoride) PVDF binder in the ratio of 80:10:10, respectively. The mixture is sonicated for 15 min to obtain a slurry with continuous homogeneity. The obtained slurry was drop cast onto 1 × 1 cm of Ni foam, followed by 12 h of vacuum-assisted drying at 60 °C.

Materials Characterization. The crystal structure and identification of phase of the prepared material was done by using powder X-ray diffraction (XRD). Scanning electron microscopy (SEM and EDX) data were taken by using a JEOL JSM-6490A. Raman spectra are obtained using a NIKON 716671 spectrometer. XPS results are obtained using a PHI Quantera SXM, and for the electrochemical analysis, a GAMRY (1010B) Potentiostat is used.

Materials Used. The MAX phase was bought from sLuoyang Tongrun Info Technology, and the phase purity was tested from XRD analysis. To remove any organic impurities of Mo_2TiAlC_2, the MAX phase was treated with HCL and dried before HF etching. MWCNTs (battery-graded) were bought from Linyi Gelon libco. Ltd. (Shandong China). CTAB was provided by Sigma-Aldrich in powder form with purity mentioned greater than 99%. HF used for etching purposes was also bought from Sigma-Aldrich with a concentration of 48%. DI water was provided by a local vendor with Ph maintained on 7 at 25 °C.

■ ASSOCIATED CONTENT

Data Availability Statement

The data will be available on demand.

■ AUTHOR INFORMATION

Corresponding Author

Syed Rizwan − *Physics Characterization and Simulations Lab (PCSL), Department of Physics, School of Natural Sciences (SNS), National University of Sciences and Technology (NUST), Islamabad 54000, Pakistan;* orcid.org/0000-0002-6934-0949; Email: syedrizwan@sns.nust.edu.pk

Authors

M. Waqas Hakim − *Physics Characterization and Simulations Lab (PCSL), Department of Physics, School of Natural Sciences (SNS), National University of Sciences and Technology (NUST), Islamabad 54000, Pakistan;* orcid.org/0000-0002-6538-3909

Irfan Ali − *Physics Characterization and Simulations Lab (PCSL), Department of Physics, School of Natural Sciences (SNS), National University of Sciences and Technology (NUST), Islamabad 54000, Pakistan*

Sabeen Fatima − *Physics Characterization and Simulations Lab (PCSL), Department of Physics, School of Natural Sciences (SNS), National University of Sciences and Technology (NUST), Islamabad 54000, Pakistan*

Hu Li − *Shandong Technology Center of Nanodevices and Integration, School of Microelectronics, Shandong University, Jinan 250101, China; Department of Material Science and Engineering, Uppsala University, 75121 Uppsala, Sweden;* orcid.org/0000-0003-1050-8441

Syed Hassan Mujtaba Jafri − *Department of Electrical Engineering, Mirpur University of Science and Technology (MUST), Mirpur 10250, Pakistan*

Complete contact information is available at: https://pubs.acs.org/10.1021/acsomega.3c04932

Author Contributions

M. Waqas Hakim performed the experimentation and testing and wrote the manuscript, Irfan Ali and Sabeen Fatima helped in understanding and reviewing, Hu Li and S. H. M. Jafri performed XPS analysis, and Syed Rizwan supervised and helped in completing the project.

Notes

The authors declare no competing financial interest.

■ ACKNOWLEDGMENTS

The authors thank the Higher Education Commission (HEC) of Pakistan for providing research funding under project no.: 20-14784/NRPU/R&D/HEC/2021. The authors also acknowledge the financial support from the Shandong Provincial Natural Science Foundation (grant no.: ZR2021QE148) and the Shandong Provincial Natural Science Foundation for Excellent Young Scientists Fund Program (Overseas) (grant no.: 2022HWYQ-060).

■ REFERENCES

(1) Lu, Z.; Raad, R.; Safaei, F.; Xi, J.; Liu, Z.; Foroughi, J. Carbon Nanotube Based Fiber Supercapacitor as Wearable Energy Storage. *Front. Mater.* **2019**, *6*, 138.

(2) Zhang, L. L.; Zhou, R.; Zhao, X. S. Graphene-Based Materials as Supercapacitor Electrodes. *J. Mater. Chem.* **2010**, *20* (29), 5983−5992.

(3) Huang, Y.; et al. Magnetic-Assisted, Self-Healable, Yarn-Based Supercapacitor. *ACS nano* **2015**, *9*, 6242.

(4) Gogotsi, Y.; Xu, M. Carbon Nanotube Composite Electrodes for High-Rate Electrochemical Energy Storage. *Nat. Commun.* **2020**, *11*, 6160.

(5) Waqas Hakim, M.; Fatima, S.; Rizwan, S.; Mahmood, A. *Pseudo-Capacitors: Introduction, Controlling Factors and Future*; Thomas, S., Ed.; Springer Nature Switzerland, 2022; pp 53−70..

(6) Chmiola, J.; Yushin, G.; Dash, R.; Gogotsi, Y. Effect of Pore Size and Surface Area of Carbide Derived Carbons on Specific Capacitance. *J. Power Sources* **2006**, *158* (1), 765−772.

(7) Li, J.; Cheng, X.; Shashurin, A.; Keidar, M. Review of Electrochemical Capacitors Based on Carbon Nanotubes and Graphene. *Graphene* **2012**, *01* (01), 1−13.

(8) Bo, Z.; Mao, S.; Jun Han, Z.; Cen, K.; Chen, J.; Ostrikov, K. Emerging Energy and Environmental Applications of Vertically-Oriented Graphenes. *Chem. Soc. Rev.* **2015**, *44* (8), 2108−2121.

(9) Pomerantseva, E.; Gogotsi, Y. Two-Dimensional Heterostructures for Energy Storage. *Nat. Energy* **2017**, *2* (7), 17089−17096.

(10) Anasori, B.; Lukatskaya, M. R.; Gogotsi, Y. 2D Metal Carbides and Nitrides (MXenes) for Energy Storage. *Nat. Rev. Mater.* **2017**, *2* (2), 16098.

(11) Liu, L.; Niu, Z.; Chen, J. Unconventional Supercapacitors from Nanocarbon-Based Electrode Materials to Device Configurations. *Chem. Soc. Rev.* **2016**, *45* (15), 4340−4363.

(12) Niu, Z.; Zhang, L.; Liu, L.; Zhu, B.; Dong, H.; Chen, X. All-Solid-State Flexible Ultrathin Micro-Supercapacitors Based on Graphene. *Adv. Mater.* **2013**, *25* (29), 4035−4042.

(13) Cui, Y.; Wu, F.; Wang, J.; Wang, Y.; Shah, T.; Liu, P.; Zhang, Q.; Zhang, B. Three Dimensional Porous MXene/CNTs Micro-

spheres: Preparation, Characterization and Microwave Absorbing Properties. *Composites, Part A* **2021**, *145*, 106378.
(14) Anasori, B.; Xie, Y.; Beidaghi, M.; Lu, J.; Hosler, B. C.; Hultman, L.; Kent, P. R. C.; Gogotsi, Y.; Barsoum, M. W. Two-Dimensional, Ordered, Double Transition Metals Carbides (MXenes). *ACS Nano* **2015**, *9* (10), 9507−9516.
(15) Lin, Z.; Barbara, D.; Taberna, P. L.; Van Aken, K. L.; Anasori, B.; Gogotsi, Y.; Simon, P. Capacitance of Ti3C2Tx MXene in Ionic Liquid Electrolyte. *J. Power Sources* **2016**, *326*, 575−579.
(16) Tahir, R.; Zahra, S. A.; Naeem, U.; Akinwande, D.; Rizwan, S. First Observation on Emergence of Strong Room-Temperature Ferroelectricity and Multiferroicity in 2D-Ti3C2Tx Free-Standing MXene Film. *RSC Adv.* **2022**, *12* (38), 24571−24578.
(17) Naguib, M.; Mochalin, V. N.; Barsoum, M. W.; Gogotsi, Y. 25th Anniversary Article: MXenes: A New Family of Two-Dimensional Materials. *Adv. Mater.* **2014**, *26* (7), 992−1005.
(18) Naguib, M.; Kurtoglu, M.; Presser, V.; Lu, J.; Niu, J.; Heon, M.; Hultman, L.; Gogotsi, Y.; Barsoum, M. W. Two-Dimensional Nanocrystals Produced by Exfoliation of Ti 3AlC 2. *Adv. Mater.* **2011**, *23* (37), 4248−4253.
(19) Ghidiu, M.; Lukatskaya, M. R.; Zhao, M. Q.; Gogotsi, Y.; Barsoum, M. W. Conductive Two-Dimensional Titanium Carbide "clay" with High Volumetric Capacitance. *Nature* **2014**, *516* (7529), 78−81.
(20) Seh, Z. W.; Fredrickson, K. D.; Anasori, B.; Kibsgaard, J.; Strickler, A. L.; Lukatskaya, M. R.; Gogotsi, Y.; Jaramillo, T. F.; Vojvodic, A. Two-Dimensional Molybdenum Carbide (MXene) as an Efficient Electrocatalyst for Hydrogen Evolution. *ACS Energy Lett.* **2016**, *1* (3), 589−594.
(21) Halim, J.; Kota, S.; Lukatskaya, M. R.; Naguib, M.; Zhao, M. Q.; Moon, E. J.; Pitock, J.; Nanda, J.; May, S. J.; Gogotsi, Y.; Barsoum, M. W. Synthesis and Characterization of 2D Molybdenum Carbide (MXene). *Adv. Funct. Mater.* **2016**, *26* (18), 3118−3127.
(22) Ali, I.; Haider, Z.; Rizwan, S. Enhanced Pseudocapacitive Energy Storage and Thermal Stability of Sn 2+ Ion-Intercalated Molybdenum Titanium Carbide (Mo 2 TiC 2) MXene. *RSC Adv.* **2022**, *12* (49), 31923−31934.
(23) Hakim, M. W.; Fatima, S.; Tahir, R.; Iqbal, M. Z.; Li, H.; Rizwan, S. Ni-Intercalated Mo2TiC2Tx Free-Standing MXene for Excellent Gravimetric Capacitance Prepared via Electrostatic Self-Assembly. *J. Energy Storage* **2023**, *61*, 106662.
(24) Jiao, S.; Zhou, A.; Wu, M.; Hu, H. Kirigami Patterning of MXene/Bacterial Cellulose Composite Paper for All-Solid-State Stretchable Micro-Supercapacitor Arrays. *Adv. Sci.* **2019**, *6* (12), 1900529.
(25) Cheng, W.; Fu, J.; Hu, H.; Ho, D. Interlayer Structure Engineering of MXene-Based Capacitor-Type Electrode for Hybrid Micro-Supercapacitor toward Battery-Level Energy Density. *Adv. Sci.* **2021**, *8* (16), 1−13.
(26) Fan, Z.; Wang, Y.; Xie, Z.; Wang, D.; Yuan, Y.; Kang, H.; Su, B.; Cheng, Z.; Liu, Y. Modified MXene/Holey Graphene Films for Advanced Supercapacitor Electrodes with Superior Energy Storage. *Adv. Sci.* **2018**, *5* (10), 1800750.
(27) Zahra, S. A.; Ceesay, E.; Rizwan, S. Zirconia-Decorated V2CTx MXene Electrodes for Supercapacitors. *J. Energy Storage* **2022**, *55*, 105721.
(28) Fan, Z.; Wang, Y.; Xie, Z.; Xu, X.; Yuan, Y.; Cheng, Z.; Liu, Y. A Nanoporous MXene Film Enables Flexible Supercapacitors with High Energy Storage. *Nanoscale* **2018**, *10* (20), 9642−9652.
(29) Shen, C.; Wang, L.; Zhou, A.; Wang, B.; Wang, X.; Lian, W.; Hu, Q.; Qin, G.; Liu, X. Synthesis and Electrochemical Properties of Two-Dimensional RGO/Ti3 C2 Tx Nanocomposites. *Nanomaterials* **2018**, *8* (2), 80.
(30) Bao, W.; Tang, X.; Guo, X.; Choi, S.; Wang, C.; Gogotsi, Y.; Wang, G. Porous Cryo-Dried MXene for Efficient Capacitive Deionization. *Joule* **2018**, *2* (4), 778−787.
(31) Liu, Y. T.; Zhang, P.; Sun, N.; Anasori, B.; Zhu, Q. Z.; Liu, H.; Gogotsi, Y.; Xu, B. Self-Assembly of Transition Metal Oxide Nanostructures on MXene Nanosheets for Fast and Stable Lithium Storage. *Adv. Mater.* **2018**, *30* (23), 1−9.
(32) Li, L.; Zhang, N.; Zhang, M.; Wu, L.; Zhang, X.; Zhang, Z. Ag-Nanoparticle-Decorated 2D Titanium Carbide (MXene) with Superior Electrochemical Performance for Supercapacitors. *ACS Sustain. Chem. Eng.* **2018**, *6* (6), 7442−7450.
(33) Yu, P.; Cao, G.; Yi, S.; Zhang, X.; Li, C.; Sun, X.; Wang, K.; Ma, Y. Binder-Free 2D Titanium Carbide (MXene)/Carbon Nanotube Composites for High-Performance Lithium-Ion Capacitors. *Nanoscale* **2018**, *10* (13), 5906−5913.
(34) Luo, J.; Zhang, W.; Yuan, H.; Jin, C.; Zhang, L.; Huang, H.; Liang, C.; Xia, Y.; Zhang, J.; Gan, Y.; Tao, X. Pillared Structure Design of MXene with Ultralarge Interlayer Spacing for High-Performance Lithium-Ion Capacitors. *ACS Nano* **2017**, *11* (3), 2459−2469.
(35) Xie, X.; Zhao, M. Q.; Anasori, B.; Maleski, K.; Ren, C. E.; Li, J.; Byles, B. W.; Pomerantseva, E.; Wang, G.; Gogotsi, Y. Porous Heterostructured MXene/Carbon Nanotube Composite Paper with High Volumetric Capacity for Sodium-Based Energy Storage Devices. *Nano Energy* **2016**, *26*, 513−523.
(36) Cao, Z.; Hu, H.; Ho, D. Micro-Redoxcapacitor: A Hybrid Architecture Out of the Notorious Energy-Power Density Dilemma. *Adv. Funct. Mater.* **2022**, *32* (19), 1−10.
(37) Raimondo, M.; Donati, G.; Milano, G.; Guadagno, L. Hybrid Composites Based on Carbon Nanotubes and Graphene Nanosheets Outperforming Their Single-Nanofiller Counterparts. *FlatChem* **2022**, *36*, 100431.
(38) Shobin, L. R.; Manivannan, S. Silver Nanowires-Single Walled Carbon Nanotubes Heterostructure Chemiresistors. *Sens. Actuators, B* **2018**, *256*, 7−17.
(39) Liang, M.; Luo, B.; Zhi, L. Application of Graphene and Graphene-Based Materials in Clean Energy-Related Devices. *Int. J. Energy Res.* **2009**, *33* (13), 1161.
(40) Landi, B. J.; Ganter, M. J.; Cress, C. D.; DiLeo, R. A.; Raffaelle, R. P. Carbon Nanotubes for Lithium Ion Batteries. *Energy Environ. Sci.* **2009**, *2* (6), 638−654.
(41) Wu, Y.; He, N.; Liang, G.; Zhang, C.; Liang, C.; Ho, D.; Wu, M.; Hu, H. Thick-Network Electrode: Enabling Dual Working Voltage Plateaus of Zn-Ion Micro-Battery with Ultrahigh Areal Capacity. *Adv. Funct. Mater.* **2023**, *473*, 2301734.
(42) Pan, H.; Li, J.; Feng, Y. P. Carbon Nanotubes for Supercapacitor. *Nanoscale Res. Lett.* **2010**, *5* (3), 654−668.
(43) Amin, R.; Ramesh Kumar, P.; Belharouak, I. Carbon Nanotubes: Applications to Energy Storage Devices. *Carbon Nanotubes—Redefining the World of Electronics*; IntechOpen, 2021..
(44) Zhao, M. Q.; Ren, C. E.; Ling, Z.; Lukatskaya, M. R.; Zhang, C.; Van Aken, K. L.; Barsoum, M. W.; Gogotsi, Y. Flexible MXene/Carbon Nanotube Composite Paper with High Volumetric Capacitance. *Adv. Mater.* **2015**, *27* (2), 339−345.
(45) Zahra, S. A.; Anasori, B.; Iqbal, M. Z.; Ravaux, F.; Al Tarawneh, M.; Rizwan, S. Enhanced Electrochemical Performance of Vanadium Carbide MXene Composites for Supercapacitors. *APL Mater.* **2022**, *10*(6), 060901-1−060901-10..
(46) Maughan, P. A.; Bouscarrat, L.; Seymour, V. R.; Shao, S.; Haigh, S. J.; Dawson, R.; Tapia-Ruiz, N.; Bimbo, N. Pillared Mo2TiC2MXene for High-Power and Long-Life Lithium and Sodium-Ion Batteries. *Nanoscale Adv.* **2021**, *3* (11), 3145−3158.
(47) Kim, H.; Anasori, B.; Gogotsi, Y.; Alshareef, H. N. Thermoelectric Properties of Two-Dimensional Molybdenum-Based MXenes. *Chem. Mater.* **2017**, *29* (15), 6472−6479.
(48) Fatima, S.; Hakim, M. W.; Akinwande, D.; Rizwan, S. Self-Generated Double Transition-Metal Carbide MXene/Graphene Oxide Trilayered Memristors for Flexible Electronics. *Mater. Today Phys.* **2022**, *26*, 100730.
(49) Abdullah, M. P.; Zulkepli, S. A. The Functionalization and Characterization of Multi-Walled Carbon Nanotubes (MWCNTs). *AIP Conf. Proc.* **2015**, *1678*..
(50) Presser, V.; Naguib, M.; Chaput, L.; Togo, A.; Hug, G.; Barsoum, M. W. First-Order Raman Scattering of the MAX Phases: Ti

https://doi.org/10.1021/acsomega.3c04932
ACS Omega 2024, 9, 8763−8772

2AlN, Ti 2AlC 0.5N 0.5, Ti 2AlC, (Ti 0.5V 0.5) 2AlC, V 2AlC, Ti 3AlC 2, and Ti 3GeC 2. *J. Raman Spectrosc.* **2012**, *43* (1), 168−172.
(51) Liu, F.; Zhou, A.; Chen, J.; Zhang, H.; Cao, J.; Wang, L.; Hu, Q. Preparation and Methane Adsorption of Two-Dimensional Carbide Ti2C. *Adsorption* **2016**, *22* (7), 915−922.
(52) Syamsai, R.; Rodriguez, J. R.; Pol, V. G.; Van Le, Q.; Batoo, K. M.; Adil, S. F.; Pandiaraj, S.; Muthumareeswaran, M. R.; Raslan, E. H.; Grace, A. N. Double Transition Metal MXene (TixTa4-xC3) 2D Materials as Anodes for Li-Ion Batteries. *Sci. Rep.* **2021**, *11* (1), 688−713.
(53) Kister, G.; Cassanas, G.; Bergounhon, M.; Hoarau, D.; Vert, M. Structural Characterization and Hydrolytic Degradation of Solid Copolymers of D, L-Lactide-Co-ε-Caprolactone by Raman Spectroscopy. *Polymer* **2000**, *41* (3), 925−932.
(54) Sarycheva, A.; Gogotsi, Y. Raman Spectroscopy Analysis of the Structure and Surface Chemistry of $Ti_3C_2T_x$ MXene. *Chem. Mater.* **2020**, *32* (8), 3480−3488.
(55) Zdrojek, M.; Gebicki, W.; Jastrzebski, C.; Melin, T.; Huczko, A. Studies of Multiwall Carbon Nanotubes Using Raman Spectroscopy and Atomic Force Microscopy. *Solid State Phenom.* **2004**, *99*−*100*, 265−268.
(56) Halim, J.; Cook, K. M.; Naguib, M.; Eklund, P.; Gogotsi, Y.; Rosen, J.; Barsoum, M. W. X-Ray Photoelectron Spectroscopy of Select Multi-Layered Transition Metal Carbides (MXenes). *Appl. Surf. Sci.* **2016**, *362*, 406−417.
(57) Halim, J.; Cook, K. M.; Eklund, P.; Rosen, J.; Barsoum, M. W. XPS of Cold Pressed Multilayered and Freestanding Delaminated 2D Thin Films of Mo2TiC2Tz and Mo2Ti2C3Tz (MXenes). *Appl. Surf. Sci.* **2019**, *494*, 1138−1147.
(58) Natu, V.; Benchakar, M.; Canaff, C.; Habrioux, A.; Célérier, S.; Barsoum, M. W. A Critical Analysis of the X-Ray Photoelectron Spectra of Ti3C2Tz MXenes. *Matter* **2021**, *4* (4), 1224−1251.
(59) Kalambate, P. K.; Dhanjai; Sinha, A.; Sinha, A.; Li, Y.; Shen, Y.; Huang, Y. An Electrochemical Sensor for Ifosfamide, Acetaminophen, Domperidone, and Sumatriptan Based on Self-Assembled MXene/MWCNT/Chitosan Nanocomposite Thin Film. *Microchim. Acta* **2020**, *187* (7), 402.
(60) Ivanova, M. V.; Lamprecht, C.; Jimena Loureiro, M.; Torin Huzil, J.; Foldvari, M. Pharmaceutical Characterization of Solid and Dispersed Carbon Nanotubes as Nanoexcipients. *Int. J. Nanomed.* **2012**, *7*, 403−415.
(61) Liu, X. M.; Huang, Z.; Oh, S. w.; Zhang, B.; Ma, P. C.; Yuen, M. M. F.; Kim, J. K. Carbon Nanotube (CNT)-Based Composites as Electrode Material for Rechargeable Li-Ion Batteries: A Review. *Compos. Sci. Technol.* **2012**, *72* (2), 121−144.
(62) Cheng, Q.; Tang, J.; Ma, J.; Zhang, H.; Shinya, N.; Qin, L. C. Graphene and Carbon Nanotube Composite Electrodes for Supercapacitors with Ultra-High Energy Density. *Phys. Chem. Chem. Phys.* **2011**, *13* (39), 17615−17624.
(63) Alnoor, H.; Elsukova, A.; Palisaitis, J.; Persson, I.; Tseng, E. N.; Lu, J.; Hultman, L.; Persson, P. O. Exploring MXenes and their MAX phase precursors by electron microscopy. *Mater. Today Adv.* **2021**, *9*, 100123.
(64) Krishnan, P.; Biju, V. Effect of Electrolyte Concentration on the Electrochemical Performance of RGO-KOH Supercapacitor. *Bull. Mater. Sci.* **2021**, *44* (4), 288.
(65) Denmark, I.; Macchi, S.; Watanabe, F.; Viswanathan, T.; Siraj, N. Effect of KOH on the Energy Storage Performance of Molasses-Based Phosphorus and Nitrogen Co-Doped Carbon. *Electrochem* **2021**, *2* (1), 29−41.
(66) Li, H.; Chen, R.; Ali, M.; Lee, H.; Ko, M. J. In Situ Grown MWCNTs/MXenes Nanocomposites on Carbon Cloth for High-Performance Flexible Supercapacitors. *Adv. Funct. Mater.* **2020**, *30* (47), 1−12.
(67) Xiao, J.; Wen, J.; Zhao, J.; Ma, X.; Gao, H.; Zhang, X. A Safe Etching Route to Synthesize Highly Crystalline Nb2CTx MXene for High Performance Asymmetric Supercapacitor Applications. *Electrochim. Acta* **2020**, *337*, 135803.
(68) Xu, W.; Xu, Z.; Liang, Y.; Liu, L.; Weng, W. Enhanced Tensile and Electrochemical Performance of MXene/CNT Hierarchical Film. *Nanotechnology* **2021**, *32* (35), 355706.
(69) Hwang, H.; Byun, S.; Yuk, S.; Kim, S.; Song, S. H.; Lee, D. High-Rate Electrospun Ti3C2Tx MXene/Carbon Nanofiber Electrodes for Flexible Supercapacitors. *Appl. Surf. Sci.* **2021**, *556* (April), 149710.
(70) Zahra, S. A.; Anasori, B.; Iqbal, M. Z.; Ravaux, F.; Al Tarawneh, M.; Rizwan, S. Enhanced Electrochemical Performance of Vanadium Carbide MXene Composites for Supercapacitors Enhanced Electrochemical Performance of Vanadium Carbide MXene Composites for Supercapacitors. *APL Mater.* **2022**, *10*, 060901.
(71) Zheng, T.; Zhang, X.; Li, Y.; Zhu, Y.; Yan, W.; Zhao, Z.; Zhang, L.; Bai, C.; Wang, X. Wet-Spinning of Continuous Hyaluronic-Based MXene/CNTs Hybrid Fibers for Flexible Supercapacitor Applications. *Mater. Lett.* **2023**, *336*, 133891.
(72) Luo, W.; Liu, Q.; Zhang, B.; Li, J.; Li, R.; Li, T.; Sun, Z.; Ma, Y. Binder-Free Flexible Ti3C2Tx MXene/Reduced Graphene Oxide/Carbon Nanotubes Film as Electrode for Asymmetric Supercapacitor. *Chem. Eng. J.* **2023**, *474*, 145553.
(73) Wang, H.; Pilon, L. Physical Interpretation of Cyclic Voltammetry for Measuring Electric Double Layer Capacitances. *Electrochim. Acta* **2012**, *64*, 130−139.
(74) Pal, B.; Yang, S.; Ramesh, S.; Thangadurai, V.; Jose, R. Electrolyte Selection for Supercapacitive Devices: A Critical Review. *Nanoscale Adv.* **2019**, *1* (10), 3807−3835.
(75) Drummond, R.; Huang, C.; Grant, P. S.; Duncan, S. R. Overcoming Diffusion Limitations in Supercapacitors Using Layered Electrodes. *J. Power Sources* **2019**, *433*, 126579.

https://doi.org/10.1021/acsomega.3c04932
ACS Omega 2024, 9, 8763−8772